CHARACTERISATION OF A STEADY STATE MPD THRUSTER WITH RADIATION COOLED ANODE

Michael Winter, Monika Auweter-Kurtz, Christian Boie, Jörg Heiermann, Helmut L. Kurtz
Institut für Raumfahrtsysteme, Universität Stuttgart
Pfaffenwaldring 31, D-70550 Stuttgart, Germany
Tel: 49-711-685-2375
email: winter@irs.uni-stuttgart.de
http://www.irs.uni-stuttgart.de

Abstract

A nozzle type stationary self-field magnetoplasmadynamic (MPD) thruster in the high power range of 100 kW up to 500 kW with radiation cooled anode was investigated at different current levels and with different mass flow rates. For this investigation argon was used as propellant. Emission spectroscopic measurements of the free flow regime were performed at a mass flow rate of 0.8 g/s and at different distances to the anode to determine excitation temperatures of the different ionization stages. These results and the main characteristics of the thruster are compared with those of a pure water-cooled version and with numerical simulations for this thruster geometry.

Introduction

Since several years extensive investigations have been carried out at the Institut für Raumfahrtsysteme (IRS) of the University of Stuttgart on self-field magnetoplasmadynamic (MPD) thrusters in the high power range of 100 kW up to 1 MW. A broad spectrum of plasma accelerators were examined, all operated in steady state mode [1, 2, 3]. The experimental work is accompanied by the development of numerical codes, allowing a theoretical calculation of the MPD thrusters and a comparison with experimental data [4, 5]. To investigate the effect of a glowing anode on thrust efficiency, thruster characteristics and especially on onset phenomena, observed at nozzle type MPD thrusters, an MPD thruster with radiation cooled anode (hot anode thruster - HAT) has been developed [1, 3], based on the water cooled DT2 thruster which is a hybrid between thermal thrusters and pure MPDs. Figures 1 and 2 show the geometries of the DT2- and the HAT thruster.

Cathode and neutral segments are still water cooled, the nozzle throat region and the combustion chamber have the same geometry like the DT2 thruster. The anode is made of thoriated tungsten, its surface is partly coated with TaC to increase the emissivity.

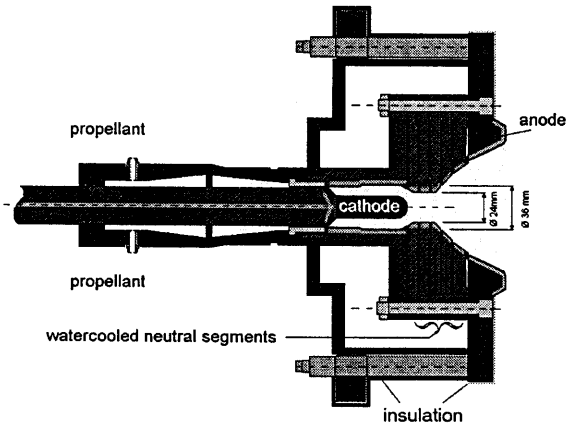

Figure 1: DT2 thruster geometry

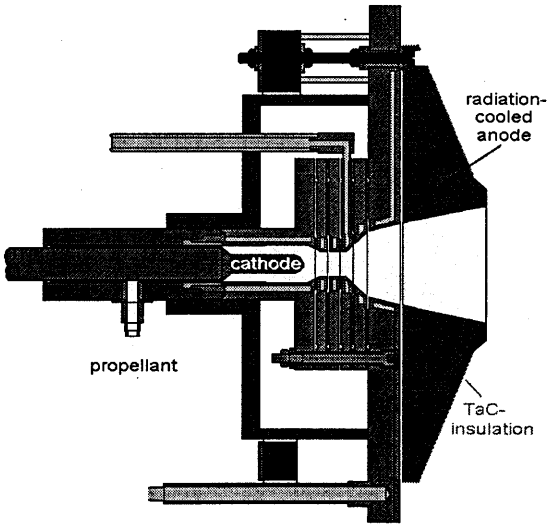

Figure 2: HAT thruster geometry

In a former investigation [3], preliminary measurements with this thruster have been performed but a broken cooling channel caused severe damage to the anode surface before thrust measurements and plasma diagnostics could be performed. In the following, these measurements are referred to as phase 1.

After the TaC coating of the anode renewed, the HAT thruster was mounted on the thrust balance of the water-cooled types and further measurements (phase 2) were carried out. The voltage values measured before the damage of the anode surface (phase 1) [3] were generally lower than those determined with the renewed anode coating (phase 2).

The heat losses at the water-cooled neutral segments are determined by measuring the temperature increase of the cooling water in combination with the water flow rates through the different segments. The axial profile of the specific heat flux provides information about the arc shape inside the thruster. It is also used for the determination of thrust efficiency.

In addition to the voltage current characteristic, the potential differences of the neutral segments to the cathode potential are measured in each test for a better understanding of the processes inside the thruster.

Parallel to the perfomance data aquisition, emission spectroscopic measurements in different cross sections of the plasma jet are performed. Radial profiles of excitation temperatures of the different ionized species are determined and compared with numerically calculated electron temperatures. From this comparison, information about the equilibrium state of the plasma can be given [6 - 8]. For time reasons, up to now only measurements of the anode exit plane have been completed.

Performance data of the thrusters

The main characteristic of these thrusters is given by the voltage-current characteristic as shown in Figure 3 in comparison to the data of the DT2 thruster and some results of the numerical simulation. The agreement between measurement and simulation is rather good. For both thrusters, the simulated voltage at 4000 A is in better agreement with the measurements than at 2000 A. The voltage level of the HAT thruster at comparable currents is higher than for the DT2 thruster.

One severe problem with the stationary nozzle type MPD thrusters is caused by instabilities starting at a critical current level which limit exhaust velocity and thrust efficiency as described in detail in [2]. These onset phenomea are indicated by a steep increase in voltage with rising current which is followed by voltage oscillations and local onsets of the arc at the anode surface yielding a destruction of the anode. Figure 4 gives an example for the critical voltage current behavior of both thruster versions at a mass flow rate of 0.3 g/s argon measured in phase 1.

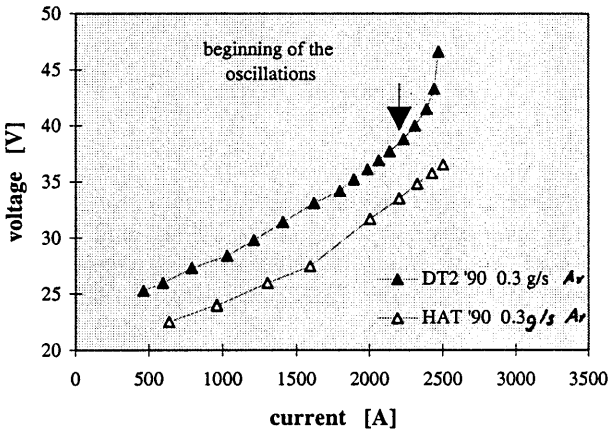

Figure 4: Voltage -current characteristic of the HAT and DT2 thruster at a mass flow rate of 0,8 g/s Ar.

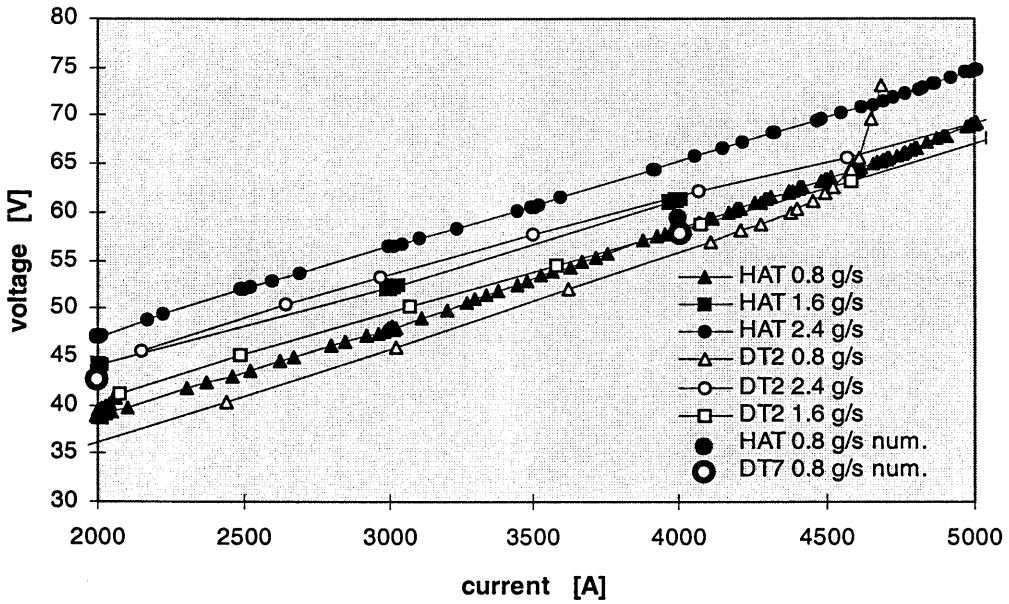

Figure 3: Voltage-current characteristic of the HAT and DT2 thruster at different argon mass flow rates

The critical voltage increase at the DT2 thruster can be seen at a current level of 2000 A, the voltage oscillations start at 2500 A. At this level the shape of the voltage current graph of the HAT thruster is comparatively flat which indicates that with the HAT thruster the instabilities occur at higher current levels, if ever. Within phase 2, the same measurements were carried out for a mass flow of 0.8 g/s argon as shown in Fig. 5. The critical current can be seen with the DT2 thruster between 4000 A and 4700 A. Again, the voltage-current characteristic of the HAT thruster does not show any signs of beginning instabilities.

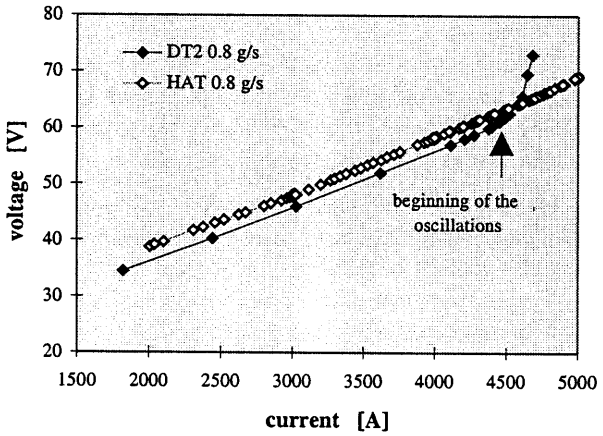

Figure 5: Voltage-current characteristic of the HAT and DT2 thruster at a mass flow rate of 0,8 g/s argon.

The potential differences of the neutral segments to the cathode give more information about the processes inside the thruster, where diagnostic investigations are hard to perform.

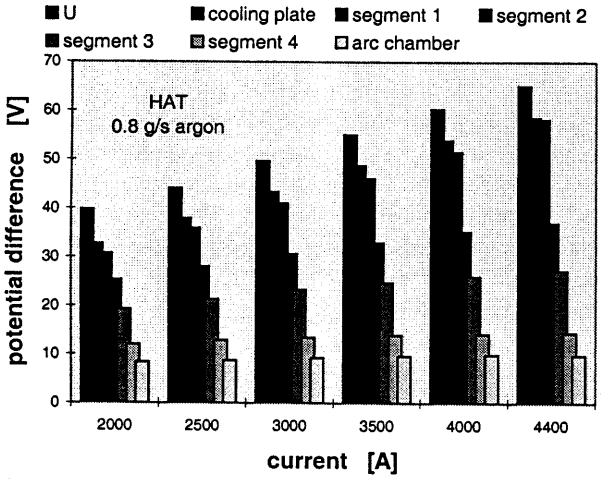

Figure 6: Potential difference of the different neutral thruster segments to the cathode

Figure 6 shows these potential differences. All potential differences rise with rising voltage but the values inside the thruster (e.g. the plenum chamber) remain almost constant with further rising current. A normalization by the arc voltage as shown in Fig. 7 demonstrates these tendencies more clearly. All potential differences decrease relative to the arc voltage with rising current. The exception is given by the cooling plate and the first neutral segment which at 4400 A actually equals the potential of the cooling plate. A possible interpretation of this behavior is that the arc is driven downstream with rising current.

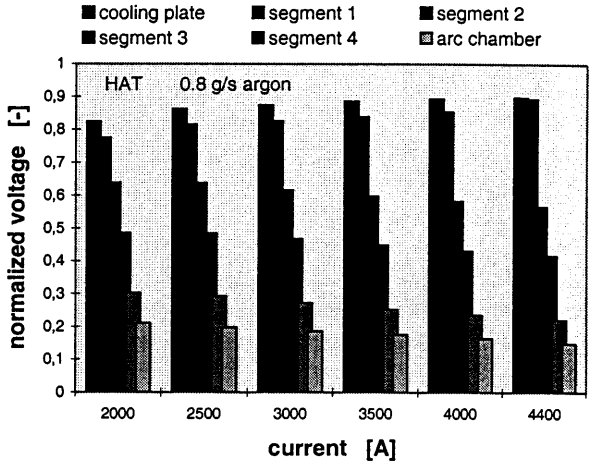

Figure 7: Potential difference to the cathode normalized by the arc voltage

Due to the heavy weight and bigger dimensions of the HAT thruster the thrust measurement stand had to be modified to perform thrust measurements. The thrust is measured by a pendulum thrust balance. The current connections are realized by mercury pots which do not disturb the movement of the thruster mount. Although the anode is shielded towards the thrust balance to minimize thermal disturbances of the thrust measurement, remarkable thermal influences on the thrust measurement can be noticed. Figure 8 shows the measured thrust at the end of the test versus time while the thruster is cooling down with no electrical power input or propellant mass flow. The fluctuations result from vibrations caused by the high pressure cooling water of the neutral segments.

To compute correction functions for the measured thrust, based on the different thermal strains of the main elements of the thrust balance, the temperatures of characteristic parts of the thrust balance have been monitored during the test. For thrust measurements with the water-cooled devices, the thruster was flexibly mounted on stainless steel edges. The rather complex geometry complicated the thermal modelling of the system. For this reason, the thrust stand was modified using stainless steel ropes instead of edges.

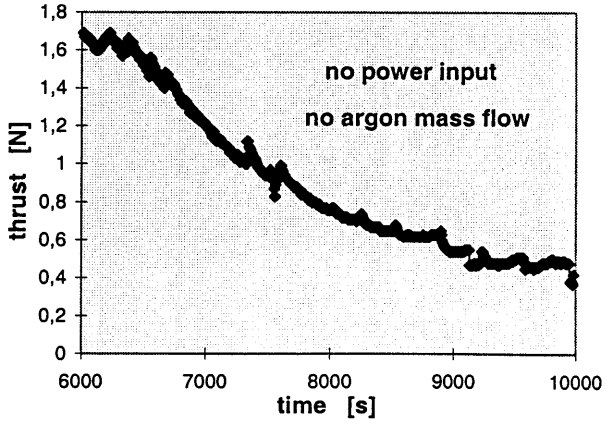

Figure 8: Thrust measurement at the end of the test

The thermal strain was determined by measuring the temperatures of both ends of the rope. First measurements showed that a linear approximation of the temperature course along the different parts of the thrust balance yielded sufficient accuracy. The principle for the temperature correction bases on the fact that the thermal strain causes components of the thruster weight in direction of the thruster axis which falsify the thrust. Due to the comparatively heavy weight of the thruster, this effect is even for small angles no longer negligible. Although the basic processes are understood, an application to the measured thrust values was not yet possible. For this reason, no thrust values can be presented here.

Numerical simulation

For comparing experimental data with computational results, the numercial code described in [7] and [8] was used to compute the electron temperature in the plasma jet. Hyperbolic-parabolic equations for the heavy particles and elliptic equations for the electron temperature and the magnetic field are solved on adaptive, unstructured grids. Equilibrium of the argon ionization reactions and thermal non-equilibrium of the electrons and the heavy particles are assumed. The cathode temperature is computed by an electrode model.

The hyperbolic-parabolic equations are solved by an explicit finite-volume solver which uses the Barth-Jesperson TVD scheme and an Osher Riemann solver. The elliptic equations are solved by triangular finite elements with linear ansatz and test functions and an SOR scheme for relaxation.

Mesh adaptation is performed using the gradient of the heavy particle temperature. The adapted primary triangulation for the Hot Anode Thruster is shown in Fig. 9.

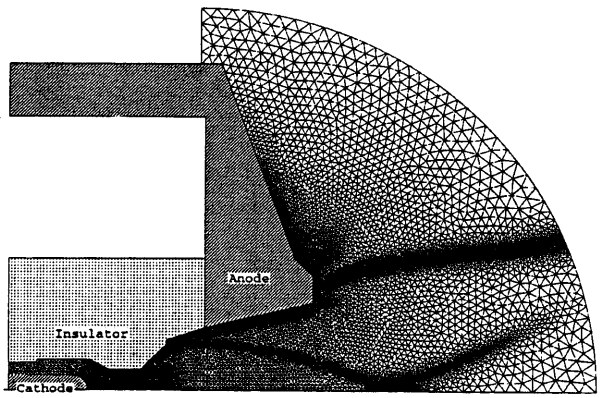

Figure 9: Adapted mesh for Hot Anode Thruster

Emission spectroscopic measurements

The measurements were done with an emission spectroscopic setup using a focussing mirror with a focal length of 660 mm and a spectrometer with a focal length of 320 mm. A detailed description of the optical setup is given in [5-7]. In each radial scan, emission lines of various ionization stages were obtained. Like already seen with the water-cooled DT7 thruster, the dominating species was single ionized argon (Ar^+) in the ultraviolet as well as in the visible wavelength region. The emission of second ionized argon (Ar^{++}) could be noticed both in the anode exit plane and at 50 mm distance to the anode, but a temperature determination yielded reasonable results only at 3000 A and 4000 A. Also the emission of neutral argon was detectable at all positions and currents.

Due to the line of sight character of emission spectroscopic measurements and the optically thin plasma, the measured intensities are integrated values. To obtain local intensities an Abel inversion has to be done. A geometrical Abel inversion was developed for this purpose as described in detail in [7].

The measured intensities have been corrected to a common intensity of a calibrated tungsten band lamp. Due to the quantitative influence of the Abel-inversion this calibration differs by an unknown but constant factor from an absolute calibration. In any case, the temperatures can be determined using relative intensities, requiring only a common calibration inside each single spectrum.

The intensity corrected emission in the different wavelength regions obtained at the anode exit plane of the HAT thruster at 4000 A and 0.8 g/s argon is given in Figs. 10 to 12. Several lines of each ionization stage have been chosen for the temperature determination according to their intensity, which had to be sufficient to assure an adequate signal to noise ratio, and according to the absence of overlapping lines referring to other excitation stages. These emission lines are marked by arrows in the presented spectra.

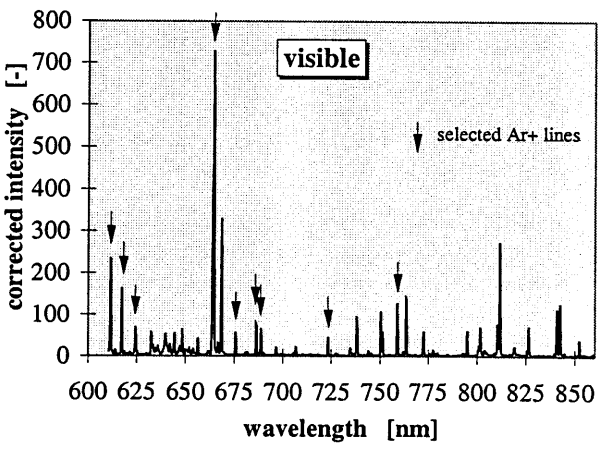

Figure 10: Typical intensity corrected emission spectrum in the visible wavelength region

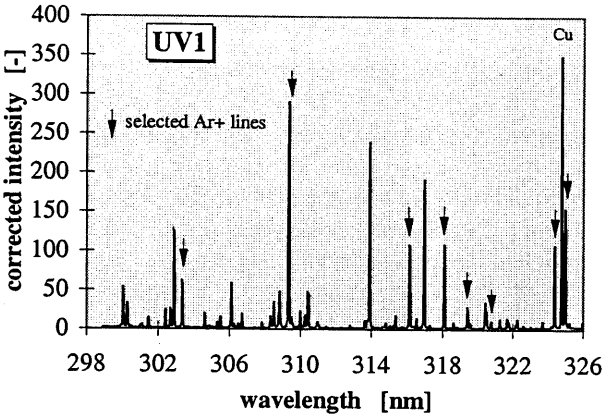

Figure 11: Typical intensity corrected emission spectrum in the UV1 wavelength region

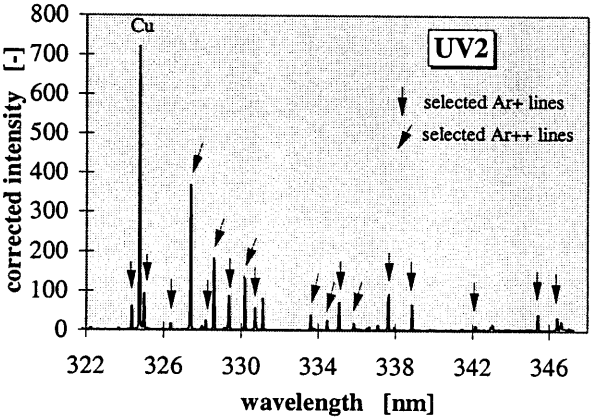

Figure 12: Typical intensity corrected emission spectrum in the UV2 wavelength region

For further interpretation, the single emission lines had to be integrated over the line width to obtain the integrated line intensities. These line intensities were Abel-inverted to obtain local intensities.

Abel Inversion Method

Due to the line of sight character of emission spectroscopic measurements and the optically thin plasma, the measured intensities are integral values. To obtain local intensities an Abel inversion has to be done. For this purpose a geometrical Abel inversion was developed to calculate a coefficient matrix for a given number of measurement points of a spheric measurement volume. This matrix describes a set of linear equations for the Abel inversion of an integrated intensity distribution and depends only on the observed geometry but not on the measured intensity values. One important assumption for a conventional Abel inversion is rotational symmetry of the plasma beam. Unfortunately, the radial characteristic of some obtained line intensities showed an asymmetrical course. In addition, the erosion of some segments indicated a concentration of the arc in the lower part of the thruster. To cover this asymmetric behavior of the thruster and to avoid discontinuities in the Abel inverted profiles, asymmetric modifications had to be added to the Abel inversion. As a result, the upper half of the plasma beam is calculated under the presumption of rotational symmetry, while in the lower half a linear transformation of the horizontal profile into the vertical profile is assumed. This technique is illustrated in Fig. 13.

A linear transformation was chosen because no concrete information about the azimuthal intensity distribution is available up to now. For future measurements an azimuthal characterisation of the plasma jet can be obtained from emission measurements from a point downstream that can be used to determine a more precise transformation method. In any case, the Abel inverted line profile seemed reasonably accurate.

In a second step, this set of linear equations is solved for a given solution vector which is represented by the measured data.

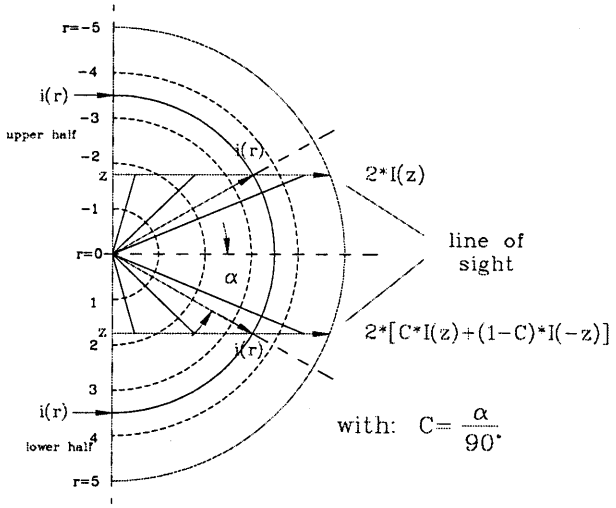

Figure 13: Model for the geometrical base of the Abel inversion

Determination of Excitation Temperatures

The total line emission coefficient ε is a function of the density n_k in the excited state k:

$$\varepsilon_L = \frac{h\nu}{4\pi} A_{ki} n_k \quad . \qquad (1)$$

Integrating the total emission coefficient along the line of sight, the intensity of a homogeneous plasma is given by

$$I_{ki} = \int \varepsilon(x)dx = \frac{h\nu}{4\pi} A_{ki} n_k l \quad , \qquad (2)$$

where l is the thickness of the emitting region. Under thermal equilibrium conditions, the density n_k is described by the Boltzmann equation:

$$n_k = \frac{g_k}{U(T_{ex})} n_0 \exp\left(-\frac{E_k}{kT_{ex}}\right) \quad , \qquad (3)$$

with the statistical weight g_k and the partition function $U(T_{ex})$. Substituting n_k in equation (2), the logarithmic equation can be obtained:

$$\ln\left(\frac{I_{ki}}{\nu A_{ki} g_k}\right) + const = -\frac{E_k}{kT_{ex}} \quad . \qquad (4)$$

The excitation temperature T_{ex} can now be determined by the relative line intensity method from the Boltzmann plots where $\ln(I_{ki}/\nu A_{ki}g_k)$ is plotted versus E_k for several emission lines belonging to the same species. The slope of the resulting straight line will be $-1/kT_{ex}$. The spectral line data as energy of upper quantum level E_k, statistical weight g_k and transition probabilities A_{ki} are taken from literature [9].

To control the resemblance of the fitted data, a correlation factor r can be defined as

$$r = \frac{\sum_{i=1}^{n}(x_i - \bar{x})(y_i - \bar{y})}{\sqrt{\sum_{i=1}^{n}(x_i - \bar{x})^2 \sum_{i=1}^{n}(y_i - \bar{y})^2}} \qquad (5)$$

$$\text{with} \quad \bar{x} = \frac{1}{n}\sum_{i=1}^{n} x_i \quad \text{and} \quad \bar{y} = \frac{1}{n}\sum_{i=1}^{n} y_i \quad . \qquad (6)$$

The probability that a linear relation is given by the measured data is high for $0.8 \le r \le 1$ and low for $0 \le r \le 0.5$. Applied to the Boltzmann plots, r gives the validity of the Boltzmann distribution. Some characteristic Boltzman plots based on Abel inverted line intensities at the center line of the thruster are presented in Fig. 14. The resulting straight line of the Boltzmann plots at one radial position shows a good correlation if the difference in exitation energy is not too small.

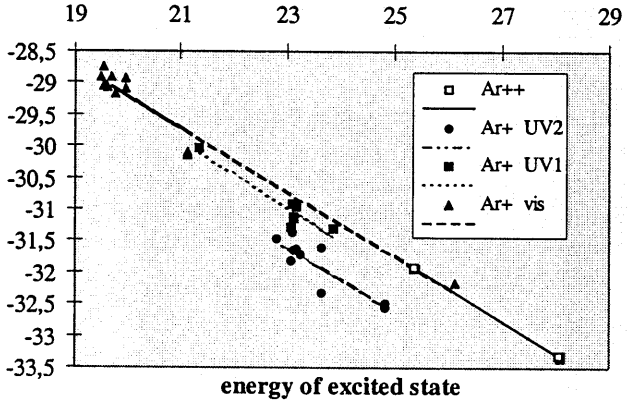

Figure 14: Boltzmann plots for the different ionization stages

COMPARISON WITH NUMERICAL RESULTS

Potential differences at the HAT thruster

The above mentioned potential differences along the thruster axis allow also a comparison with the numerical simulation inside the thruster. Figs. 15 and 16 show a comparison of the measured and computed potential differences at 2000 A and 4000 A.

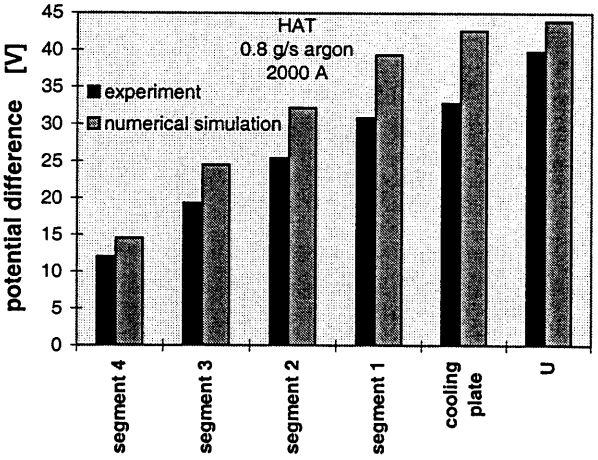

Figure 15: Measured and numerically simulated potential differences of the different neutral thruster segments to the cathode at a current of 2000 A

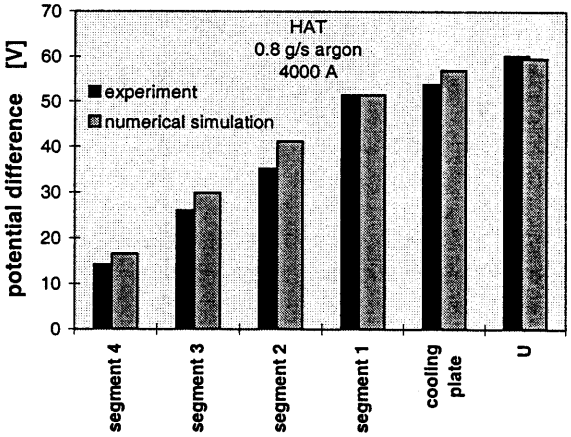

Figure 16: Measured and numerically simulated potential differences of the different neutral thruster segments to the cathode at a current of 4000 A

At 2000 A the numerically simulated segment potentials are constantly higher than the experimentally determined values. The average difference amounts to 20 %.

At 4000 A, the numerical simulation agrees well with the experiment is really good, especially in the region close to the anode.

Temperatures at the HAT thruster

In Figs. 17 and 18 the radial excitation temperature profiles of Ar, Ar^+ and Ar^{++} in the anode exit plane and at a distance of 50 mm to the anode of the HAT thruster calculated from measurements and the electron temperature obtained by the numerical simulation as described in detail in [7, 8] are plotted. The thin lines with the white symbols give the correlation factor for each corresponding Boltzmann plot.

The most obvious fact is that the excitation temperatures for Ar^+ and Ar^{++} are at least in the same range but the excitation temperature for neutral argon is remarkably lower. This leads to the conclusion that the excitation of neutral argon does not happen inside the thruster. Instead, neutral argon is the result of recirculation processes of cold gas in the vacuum tank.

Furthermore it can be noticed that the agreement between the two Ar^+ excitation temperatures becomes better with rising current. An Ar^{++} excitation temperature could not be determined at 2000 A. In the anode exit plane, even at 3000 A the temperature profiles do not indicate a Boltzmann distribution for the particle densities of the excited states. The agreement between the experimentally determined temperatures is best at 4000 A at a distance of 50 mm to the anode.

Unfortunately, no numerical data for a current of 3000 A is available at the moment but the comparison with the numerically determined temperatures for the electrons and the heavy particles at 2000 and 4000 A shows the same tendencies as the comparison of the different excitation temperatures. At 4000 A on the center axis at a distance of 50 mm to the anode exit plane the agreement between all temperatures, except of the excitation temperature for neutral argon, is almost perfect. Here, at least thermal equilibrium can be assumed

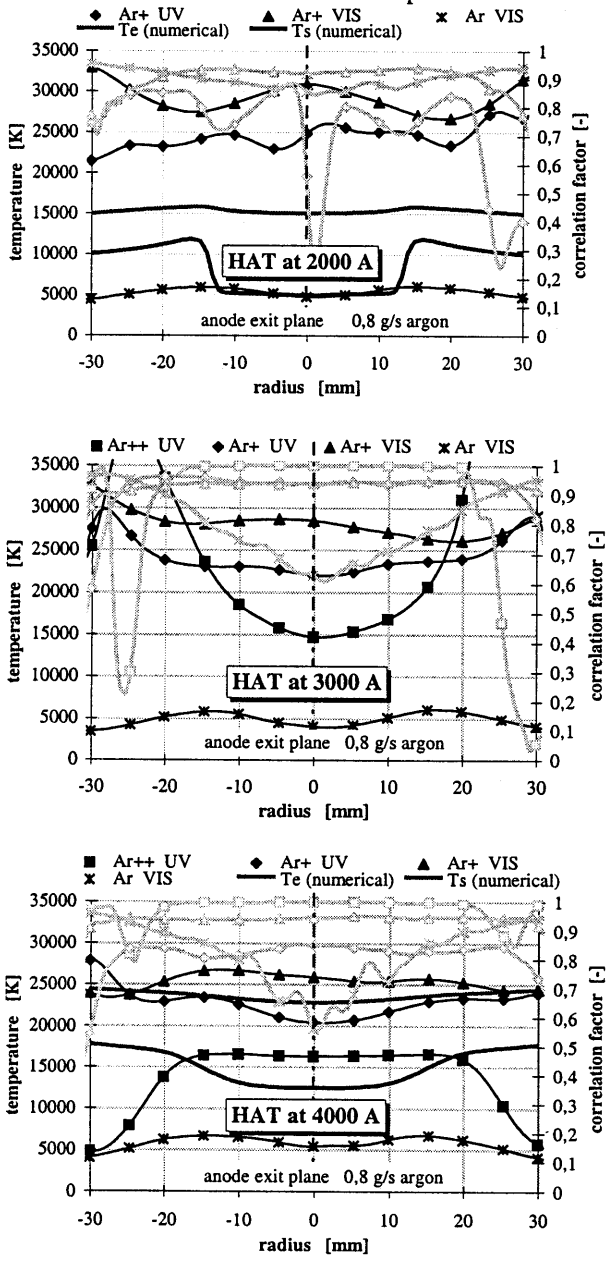

Figure 17: T_{ex}, T_e and correlation factor in the anode exit plane

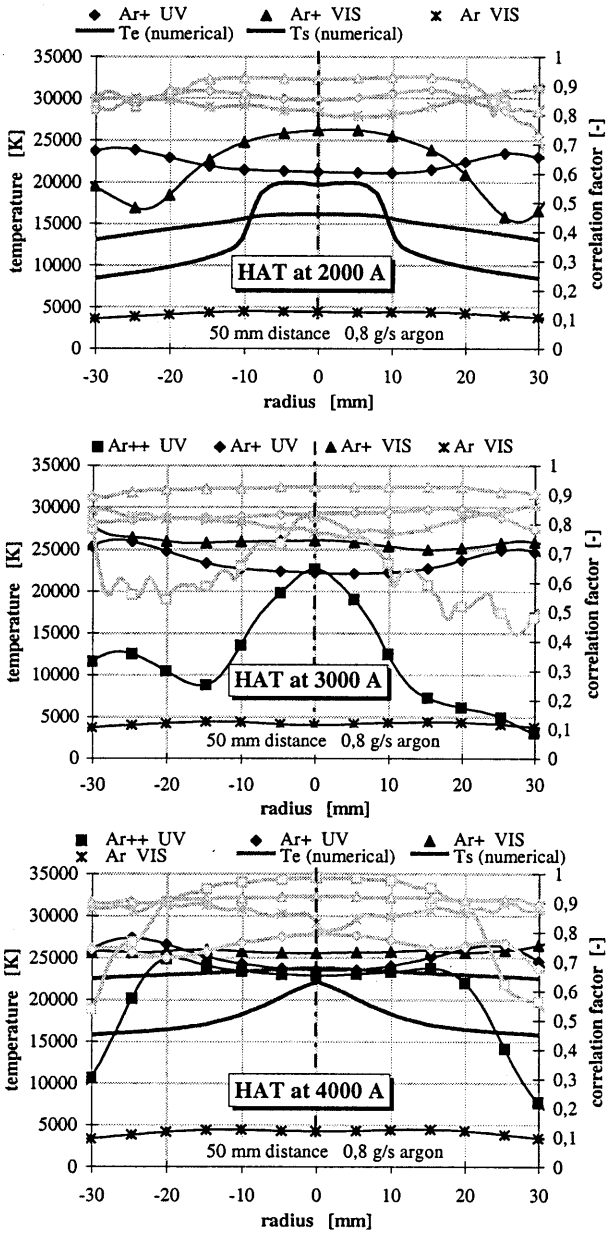

Figure 18: T_{ex}, T_e and correlation factor at 50 mm distance to the anode

Generally, it seems that the numerical simulation underestimates the electron temperature close to the anode and at low currents, even if the agreement between the experimentally determined excitation temperatures is not good enough to assume equilibrium.

Summary and future plans

A self-field MPD thruster with radiation cooled anode has been investigated. The thruster characteristics, mainly represented by the voltage-current relations have been determined. The plasma instabilities which have been observed at the water-cooled MPD thrusters could not be seen with the radiation cooled anode. Further investigations at higher current levels will show if the critical current is only shifted to higher currents or if the instabilities do not occur with the radiation cooled anode. Additional information about the region inside the thruster could be obtained from measured potential differences between the neutral segments and the cathode. A comparison with the numerical simulation showed too high values in the simulation at 2000 A and a really good agreement at 4000 A close to the anode.

The thrust measurements showed strong disturbances by thermal strain of the thrust balance. A method to correct these errors has been developed but not applied, therefore thrust values are presented.

Excitation temperatures for Ar, Ar^{+} and Ar^{++} were determined from emission spectroscopic measurements in the anode exit plane and at a distance of 50 mm to the anode. The plasma comes the closer to equilibrium the higher the current. Furthermore, the cross section at 50 mm distance to the anode is closer to equilibrium than the anode exit plane cross section. For the water-cooled thruster DT2, the anode exit plane was the cross section which was closest to equilibrium [5 - 7]. This yields the conclusion that in the HAT the arc is driven downstream in comparison to the water-cooled thruster. Again, investigations at higher current levels will show if this shift is the reason for the absence of plasma instabilities.

A comparison with numerically determined electron temperatures showed the same tendencies. Again, the agreement at 4000 A was better than at 2000 A.

In the near future, the thermal correction method for the thrust values will be completed and applied to the measured thrust values.

References

[1] Monika Auweter-Kurtz, *Plasma thruster development program at the IRS*, Acta Astronautica, Vol. 32(5): pp. 377--391, 1994.

[2] Herbert O. Schrade, Thomas Wegmann and Thomas Rösgen, *The onset phenomena explained by run-away joule heating*, IEPC 91-022, AIDAA/AIAA/DGLR/JSASS 22nd International Electric Propulsion Conference, October 14-17, 1991 / Viareggio, Italy.

[3] Th. Wegmann, *Experimentelle Untersuchung kontinuierlich betriebener magnetoplasma-dynamischer Eigenfeldtriebwerke*, Dissertation, Fakultät Luft- und Raumfahrttechnik, Universität Stuttgart, 1994.

[4] M. Auweter-Kurtz, C. Boie, H.J. Kaeppeler, H.L. Kurtz, H.O. Schrade, P.C. Sleziona, H.P. Wagner, and Th. Wegmann, *Magnetoplasmadynamic thrusters--design criteria and numerical simulation*, International Journal of Applied Electromagnetics in Materials, Vol. 4: pp. 383--401, 1994.

[5] Winter, M. W., Auweter-Kurtz, M., Boie, Ch., Kurtz, H. L., *Experimental and Numerical Investigation of Steady State MPD thrusters*, Second European Spacecraft Propulsion Conference, May 1997, Noordwijk, NL.

[6] Winter, M. W., Auweter-Kurtz, M., Boie, Ch., Kurtz, H. L., *Investigation of the Plasmastate of Steady State MPD thrusters by Emission Spectroscopic Means*, 25th International Electric Propulsion Conference, August 1997, Cleveland, OH, USA.

[7] Auweter-Kurtz, M., Boie, C., Habiger, H., Kaeppeler, H.J., Kurtz, H.L., Sleziona, P.C., Wegmann, T., Winter, M.W.: *Numerische Simulation von MPD-Triebwerken und Vergleich mit durchzuführenden experimentellen Untersuchungen*, Final Report of the DFG Research Project Au85/5-2, Institut für Raumfahrtsysteme, Universität Stuttgart, 1998.

[8] Boie, C., Auweter-Kurtz, M., Kaeppeler, H.J., Sleziona, P.C.: *Application of Adaptive Numerical Schemes for MPD Thruster Simulation*, IEPC-97-115, 25th International Electric Propulsion Conference, Cleveland, Ohio, August 1997.

[9] W. L. Wiese, M. W. Smith and B. M. Miles, *Atomic Transition Probabilities, Volume II, Sodium through Calcium*, Institute for Basic Standards, National Bureau of Standards, Washington, D. C., October 1969.